Photoemission and x-ray absorption spectroscopy study of electron-doped colossal magnetoresistive manganite $La_{0.7}Ce_{0.3}MnO_3$ films

S. W. Han[1], J.-S. Kang,[2,*] K. H. Kim,[1] J. D. Lee,[1] J. H. Kim,[2] S. C. Wi,[2] C. Mitra,[3] P. Raychaudhuri,[4] S. Wirth,[5] K. J. Kim,[6] B. S. Kim,[6] J. I. Jeong,[7] S. K. Kwon,[8] and B. I. Min[8]

[1]*Department of Physics and the Research Institute of Natural Sciences, Gyeongsang National University, Chinju 660-701, Korea*

[2]*Department of Physics, The Catholic University of Korea, Puchon 420-743, Korea*

[3]*Department of Materials Science, University of Cambridge, Pembroke Street, Cambridge CB2 3QZ, United Kingdom*

[4]*Tata Institute of Fundamental Research, Homi Bhabha Road, Bombay 400005, India*

[5]*Max Planck Institute for Chemical Physics of Solids, Nöthnizer Strasse 40, 01187 Dresden, Germany*

[6]*Pohang Accelerator Laboratory (PAL), Pohang University of Science and Technology, Pohang 790-784, Korea*

[7]*Research Institute of Industrial Science and Technology, Pohang 790-600, Korea*

[8]*Department of Physics, Pohang University of Science and Technology, Pohang 790-784, Korea*

(Received 7 September 2003; published 12 March 2004)

The electronic structure of $La_{0.7}Ce_{0.3}MnO_3$ (LCeMO) thin films has been investigated using photoemission spectroscopy (PES) and x-ray absorption spectroscopy (XAS). The Ce $3d$ core-level PES and XAS spectra of LCeMO are very similar to those of CeO_2, indicating that Ce ions are close to being tetravalent. A very weak $4f$ resonance is observed around the Ce $4d \rightarrow 4f$ absorption edge, suggesting that the localized Ce $4f$ states are almost empty in the ground state. The Mn $2p$ XAS spectrum reveals the existence of the Mn^{2+} multiplet feature, confirming the Mn^{2+}-Mn^{3+} mixed-valent states of Mn ions in LCeMO. The measured Mn $3d$ PES/XAS spectra for LCeMO agree reasonably well with the Mn $3d$ partial density of states calculated using the LSDA+U (LSDA, local spin-density approximation) method. The LSDA+U calculation predicts a half-metallic ground state for LCeMO. This study confirms that the LCeMO films are indeed electron doped.

DOI: 10.1103/PhysRevB.69.104406 PACS number(s): 79.60.−i, 75.70.−i, 71.30.+h

I. INTRODUCTION

Perovskite Mn oxides of $R_{1-x}A_xMnO_3$ (RAMO; R, rare earth; A, divalent cation) (Ref. 1) have attracted much attention due to the colossal-magnetoresistance (CMR) behavior. Pure $LaMnO_3$ is an antiferromagnetic insulator. When $LaMnO_3$ is doped with divalent cations, it undergoes a phase transition to a ferromagnetic metal, in which Mn ions can exist in the formally trivalent and tetravalent states. Zener has explained[2] the simultaneous metallic and ferromagnetic transition in RAMO in terms of the double-exchange (DE) interaction between spin-aligned Mn^{3+} ($t_{2g}^3 e_g^1$) and Mn^{4+} (t_{2g}^3) ions through oxygen ions.

In the DE model, Mn ions should exist in mixed-valent states to maintain the correlation between magnetism and conductivity. The question has been raised whether the DE mechanism is still operative when a tetravalent ion is doped instead of a divalent ion.[3] This will result in a system with Mn ions being in the Mn^{2+} ($t_{2g}^3 e_g^2$)/Mn^{3+} ($t_{2g}^3 e_g^1$) mixed-valent states. Interestingly, the metal-insulator (M-I) and ferromagnetic transitions and the concomitant CMR phenomenon have been observed in the Ce-doped manganites of $R_{0.7}Ce_{0.3}MnO_3$ (R=La,Pr,Nd).[3,4] If Ce ions in $R_{0.7}Ce_{0.3}MnO_3$ exist in the tetravalent states, Mn^{2+} ions could be formed and electronlike charge carriers would be responsible for the metallic conductivity and ferromagnetism. Therefore it is essential to know the electronic structures of $R_{0.7}Ce_{0.3}MnO_3$ in order to understand the underlying physics for the metallic ferromagnetism properly.

In our previous photoemission spectroscopy (PES) study on polycrystalline $La_{0.7}Ce_{0.3}MnO_3$ (LCeMO) bulk samples,[5] we have found that Ce ions in LCeMO are mainly in the tetravalent (4+) states, which allows the existence of the divalent Mn^{2+} ions in LCeMO. However, one of the main difficulties in this system is that the $La_{1-x}Ce_xMnO_3$ system forms in the single phase only in epitaxial thin films.[6,7] Recently, the Ce^{4+} valence state and the Mn^{2+}-Mn^{3+} mixed-valent states were observed in a thin film of LCeMO (Ref. 8) via x-ray absorption spectroscopy (XAS). Nevertheless, the detailed spectroscopic information on the electronic states near the Fermi energy E_F is lacking for LCeMO, which is important in understanding the nature of the charge carriers. In this paper, we report the PES and XAS study of LCeMO thin films. This work includes the resonant photoemission spectroscopy (RPES) measurement near the Ce $4d \rightarrow 4f$ absorption edge, and the XAS measurements near the Ce and La $3d$, Mn $2p$, and O $1s$ absorption edges. PES and XAS data have been compared to the band-structure calculations performed in the LSDA+U method (LSDA: local spin-density approximation) where U denotes the on-site Coulomb correlation interaction for both Mn $3d$ and Ce $4f$ electrons.

II. EXPERIMENTAL AND CALCULATIONAL DETAILS

The epitaxial films of $La_{0.7}Ce_{0.3}MnO_3$ were deposited on $LaAlO_3$ substrates by pulsed laser deposition at an oxygen pressure of 400 mTorr. The details of the film growth are described in Ref. 7. No impurity phase was detected from the x-ray diffraction measurement. The resistivity measurement showed a sharp and clean peak around 250 K, indicating the M-I transition. PES and XAS measurements were performed at the 2B1 beamline of the Pohang Accelerator Laboratory

(PAL). The chamber pressure was about $\sim 5\times 10^{-10}$ Torr during measurements. All spectra were obtained at room temperature. The Fermi level of the system was determined from the valence-band spectrum of an Au foil in electrical contact with samples. The overall instrumental resolution was about ~ 200 meV at a photon energy $h\nu \approx 30$ eV and ~ 300 meV at $h\nu \approx 120$ eV. To obtain clean surfaces, the samples were annealed repeatedly at $\sim 700\,^{\circ}$C in the O_2 pressure of about 1×10^{-8} Torr. The cleanliness of sample surfaces was monitored by the absence of the bump around 9-eV binding energy (BE) and the symmetrical line shape of the O $1s$ core level. All the spectra were normalized to the photon flux estimated from the mesh current.

The electronic structures of LCeMO have been calculated by employing the self-consistent linearized muffin-tin-orbital band method. To simulate the Ce-doped $LaMnO_3$ system, we considered a supercell of $La_2CeMn_3O_9$ with a tetragonal structure ($a=3.873$ Å and $c=11.618$ Å). The partial densities of states (PDOS's) for LCeMO were obtained from the LSDA$+U$ band method which incorporates the spin-orbit interaction.[9]

III. RESULT AND DISCUSSION

We first present the Ce and La $3d$ core level PES and XAS spectra of LCeMO. XAS and core-level spectroscopy are powerful methods of determining the valence states of ions in solids. In the final state of core-level PES and XAS spectra, a core hole is left behind, and it couples with valence electrons. In the systems with incompletely filled $4f$ or $3d$ electrons, the coupling between the core hole and $4f$ or $3d$ electrons is strong enough to cause the characteristic spectral splitting in XAS and XPS spectra. Therefore, by analyzing XPS and XAS, an important information on the $4f$ and $3d$ valence electrons can be obtained.

Figure 1 compares the Ce $3d$ core-level PES spectrum of LCeMO to that of CeO_2 with formally tetravalent Ce ions (Ce^{4+}) (upper panel), and the La $3d$ core-level PES spectrum of LCeMO to that of La_2O_3 with formally trivalent La ions (La^{3+}) (bottom panel). The $3d$ core-level spectra of CeO_2 and La_2O_3 were reproduced from Ref. 10 and Ref. 11, respectively. The spectrum of CeO_2 was then shifted so that the $3d_{5/2}$ main peak is aligned to that of LCeMO. These spectra exhibit the same magnitudes of the spin-orbit splittings between the $3d_{3/2}$ and $3d_{5/2}$ levels, 16.8 eV for the La $3d$ spectra and 18.1 eV for the Ce $3d$ spectra, respectively. It is clearly observed that the Ce and La $3d$ spectra of LCeMO are very similar to those of CeO_2 and La_2O_3, respectively, indicating that Ce ions in LCeMO are nearly tetravalent (Ce^{4+}) while La ions are trivalent (La^{3+}).

The solid lines along the measured $3d$ spectra for CeO_2 and La_2O_3 denote the curve-fitting results, by employing the Doniach-Sunjic line-shape function.[12] The curve-fitting analysis reveals that the Ce $3d$ PES spectrum of CeO_2 consists of six peaks, and similarly for LCeMO. These six peaks arise from the three-peak structures for each spin-orbit split component of $3d_{5/2}$ and $3d_{3/2}$, respectively. Among the three-peak structures, the highest BE components (C, C') correspond to the roughly $3d^9 4f^0$ final-state configuration.[10,13] So this figure indicates that CeO_2 and LCeMO have a very large amount of $3d^{10}4f^0$ initial-state configuration. According to the impurity Anderson Hamiltonian (IAH) analysis,[10,14] the lowest BE peaks (A, A') and the middle BE peaks (B, B') correspond to the bonding and antibonding states of the strongly mixed $3d^9 4f^1\underline{L}$ and $3d^9 4f^2\underline{L}^2$ final-state configurations ($\underline{L}$, a ligand hole). Since the charge-transfer energy Δ_f between the $4f^0$ and $4f^1\underline{L}$ configurations is small in CeO_2, the ground state is strongly mixed between $4f^0$ and $4f^1\underline{L}$ configurations. Hence the valence electronic states in CeO_2 contain non-negligible contributions from the extended states of f symmetry, even though the localized $4f$ states remain nearly unoccupied. This results in the average $4f$ electron number n_f of about 0.5 in CeO_2.

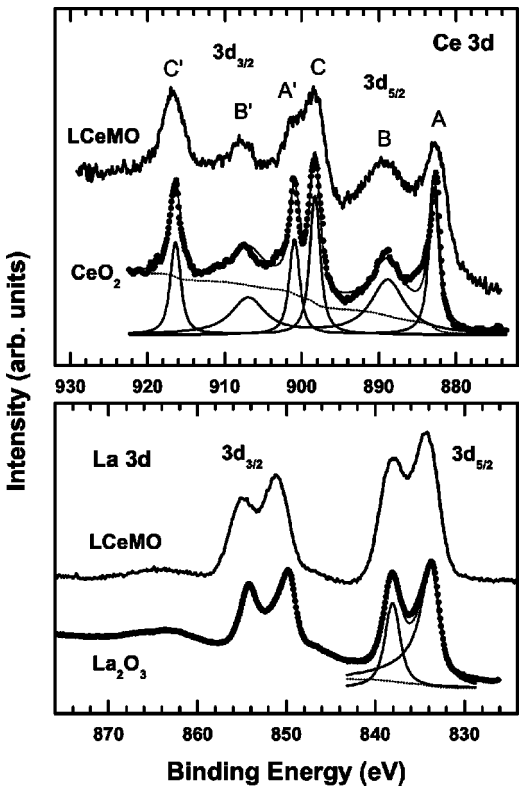

FIG. 1. Top: Comparison of the Ce $3d$ core-level PES spectra of LCeMO and CeO_2 (from Ref. 10). The curve fitting results (solid lines) of the Ce $3d$ spectrum for CeO_2 are superposed on the measured spectrum (dots). Bottom: Similarly for the La $3d$ core-level PES spectra for LCeMO and La_2O_3 (from Ref. 11).

The La $3d$ spectra show the double-peak structures of nearly equal intensity for both the $3d_{5/2}$ and $3d_{3/2}$ levels. Based on the IAH analysis,[10,14] it is well known that the La $4f$ level in the ground state of La_2O_3 is nearly empty due to the very weak hybridization between La $4f$ and O $2p$ orbitals. On the other hand, in the $3d$ core-hole final state, the attractive Coulomb interaction U_{fc} between the $3d$ core hole and the $4f$ electrons ($U_{fc}<0$) pulls down the $4f$ level, so that the charge-transfer energy Δ_f between $3d^9 4f^0$ and $3d^9 4f^1\underline{L}^1$ becomes almost vanishing, resulting in a strong hybridization between $3d^9 4f^0$ and $3d^9 4f^1\underline{L}^1$ final-state configurations. Therefore the $3d^9 4f^0$ and $3d^9 4f^1\underline{L}^1$ configura-

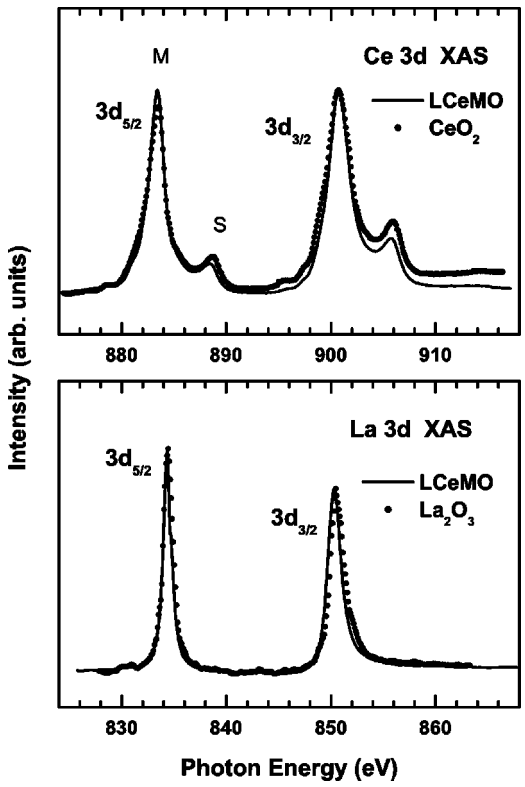

FIG. 2. Top: Comparison of the Ce $3d$ XAS spectra of LCeMO and CeO_2 (from Ref. 16). Bottom: Comparison of the La $3d$ XAS spectra of LCeMO and La_2O_3 (from Ref. 16).

tions are strongly mixed in the $3d$ core-hole final state of La_2O_3. The two peaks of the La $3d$ core level PES spectrum in La_2O_3 correspond to the bonding and antibonding states of the $3d^9 4f^0$ and $3d^9 4f^1 \underline{L}^1$ configurations. Due to the strong final-state mixing in La_2O_3, the intensities[15] of the two peaks become comparable. This interpretation can be similarly applied to the La $3d$ PES spectrum of LCeMO. Thus, Fig. 1 provides evidence that La $4f$ states are almost unoccupied in the ground state ($4f^0$), but are strongly hybridized with the O $2p$ states in the $3d$ core-hole final state.

Figure 2 shows the Ce $3d$ XAS spectra of LCeMO and CeO_2, and the La $3d$ XAS spectra of LCeMO and La_2O_3. The $3d$ XAS spectra of both CeO_2 and La_2O_3 were reproduced from Ref. 16. The Ce $3d$ XAS spectrum of LCeMO is very similar to that of CeO_2, consistent with the finding for Ce $3d$ PES spectrum, which confirms the tetravalent valency of Ce ions in LCeMO. The Ce $3d$ XAS spectra of both LCeMO and CeO_2 reveal a main peak (M) and a weak satellite (S) on the high-energy side of the main peak. The main Ce $3d$ XAS peaks show no multiplet structures. The M and S peaks correspond to the bonding and antibonding final states of the $3d^9 4f^1$ and $3d^9 4f^2 \underline{L}^1$ mixed configurations. Since the ground state $|g\rangle$ of CeO_2 will be $|g\rangle \approx \alpha|f^0\rangle + \beta|f^1 \underline{L}\rangle$, the $3d$ XAS final states will have both the $3d^9 4f^1$ and $3d^9 4f^2 \underline{L}$ configurations. In both LCeMO and CeO_2, the energy difference between M and S in the Ce $3d$ XAS spectrum (≈ 17.5 eV) is approximately the same as that between $A(A')$ and $B(B')$ in the Ce $3d$ core-level PES spectrum (≈ 18.1 eV). Note that, except for the weak satellite features, the Ce $3d$ XAS spectrum of CeO_2 is very similar to the La $3d$ XAS spectrum of La_2O_3, suggesting that the multiplet structures of the $3d$ XAS of CeO_2 resemble those of La_2O_3 with La^{3+} which has the $4f^0$ configuration in the ground state.

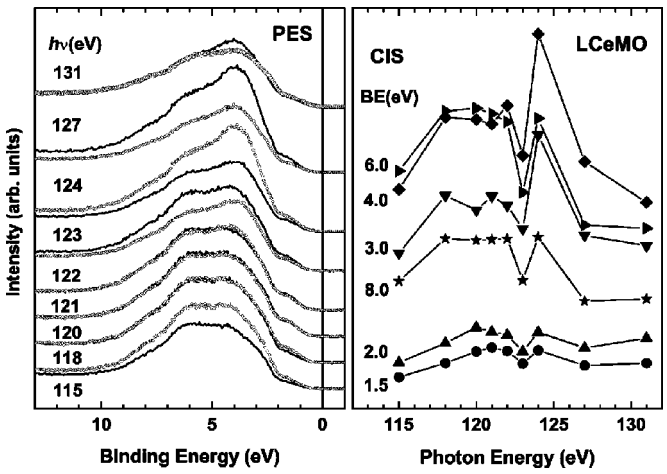

FIG. 3. Left: The valence-band spectra for LCeMO vs $h\nu$, obtained at the Ce $4d \rightarrow 4f$ absorption region. In each set of the two superposed spectra, solid lines and open circles correspond to the spectra for the lower $h\nu$ and the next higher $h\nu$, respectively. Each set of $h\nu$ values is labeled at the left side of the spectra. Right: the constant-initial-state (CIS) spectra of LCeMO for several initial states, which were obtained by plotting the photoemission intensities at several BE's vs $h\nu$.

Figure 3 presents the normalized valence-band spectra for LCeMO obtained at the Ce $4d \rightarrow 4f$ absorption region. In each set of the two superposed spectra, solid lines and open circles correspond to the spectrum for the lower $h\nu$ and that for the next higher $h\nu$. The values of $h\nu$'s are labeled at the left side of the spectra in the increasing order from bottom toward top of the figure. If there are localized Ce $4f$ electrons, the $4f$ photoemission intensity is enhanced at $h\nu \approx 121$ eV due to the resonance effect through the interference between two processes.[17] The first is the direct photoemission process, such as

$$4d^{10} 4f^n + h\nu \rightarrow 4d^{10} 4f^{n-1} \epsilon_k, \tag{1}$$

where ϵ_k denotes the emitted electron. The second is the photoabsorption of a $4d$ electron to an unoccupied $4f$ state, followed by a two-electron super Coster-Kronig Auger decay, such as

$$4d^{10} 4f^n + h\nu \rightarrow 4d^9 4f^{n+1} \rightarrow 4d^{10} 4f^{n-1} \epsilon_k. \tag{2}$$

The interference between these two processes leads to the Fano resonance. Such a RPES process will not be invoked for a tetravalent Ce^{4+} ion ($4f^0$) because there is no direct process available. Therefore the very weak enhancement around $h\nu \approx 121$ eV indicates that the localized Ce $4f$ states are nearly unoccupied in LCeMO and that the Ce valence is far from $3+$. This finding is consistent with that for the Ce $3d$ core-level PES and XAS spectra (Fig. 1 and Fig. 2).

The right panel of Fig. 3 shows $h\nu$ dependence of the emissions at several initial-state energies. These are the plots of the normalized photoemission intensities at several BEs versus $h\nu$ around the Ce $4d$ absorption thresholds. Hence these curves measure the RPES cross-section line shapes, and correspond to the constant-initial-state (CIS) spectra. In constructing the CIS spectra presented in this figure the inelastic backgrounds have not been subtracted from the valence-band spectra. The vertical scale of this figure is arbitrary but it is the same for all the spectra with different BE states.

The O $2p$ states, with BE between ~ 3 eV and ~ 8 eV, show the strong peaks around ~ 124 eV. Such a resonating behavior for the O $2p$ states agrees with that for CeO_2.[18] We interpret that this peak reflects the resonance enhancement of the extended states of f symmetry near the Ce $4d \rightarrow 4f$ absorption due to the hybridization mixing of the O $2p$ states with the Ce $4f$ states. The resonance for the O $2p$ states can occur due to the interference between the following two processes:

$$4d^{10}4f^{0}(O\ \ 2p)^{n}+h\nu \rightarrow 4d^{10}4f^{0}(O\ \ 2p)^{n-1}\epsilon_{k} \qquad (3)$$

and

$$4d^{10}4f^{0}(O\ \ 2p)^{n}+h\nu \rightarrow 4d^{9}4f^{1}(O\ \ 2p)^{n} \rightarrow 4d^{10}4f^{0}(O\ \ 2p)^{n-1}\epsilon_{k}. \qquad (4)$$

That is, the resonance occurs through the combined process of photoabsorption and the subsequent Auger decay. The intensity of the Auger process is proportional to the matrix element of the Coulomb interaction between relevant orbitals; $\langle 4d,\epsilon_k|1/r_{12}|4f,(O)2p\rangle$. Hence the resonance energies of the Ce $4f$ and O $2p$ orbitals need not necessarily be the same.[19] In the present system, the resonance energy of the hybridized O $2p$ states is expected to be higher than that of the Ce $4f$ resonance because the Ce $4f$ orbitals are located above E_F. The strong resonance of the O $2p$ states implies the large Auger matrix element, and accordingly indicates the substantial wave function overlap between the O $2p$ states and the unoccupied Ce $4f$ states. Indeed, the calculated band structure shows the non-negligible O $2p$ states above E_F hybridized with the unoccupied Ce $4f$ states as well as the extended O $2p$ states of f symmetry below E_F between -8 and -2 eV.

The low BE states, those at $1-2$ eV below E_F, show another weak peak around ~ 121 eV, which is ascribed to the resonance of the localized Ce $4f$ electrons due to the Ce $4d \rightarrow 4f$ absorption. The very weak resonance of the low BE states indicates that the localized $4f$ states are almost unoccupied in LCeMO. On the other hand, the strong resonance of the O $2p$ electrons suggests that the valence-band states contain the extended states of f symmetry, which are responsible for the non-negligible $4f$ population of n_f in its ground state ($n_f \sim 0.5$ for CeO_2). It is difficult to tell whether the resonance peak at $h\nu \sim 121$ eV for BE's $\approx 1-2$ eV has a Fano line shape. This is because the enhancement is very weak and it overlaps with the strong La $5d$ resonance due to the La $4d \rightarrow 4f$ RPES, which has a broad maximum around $h\nu = 118-122$ eV.[5]

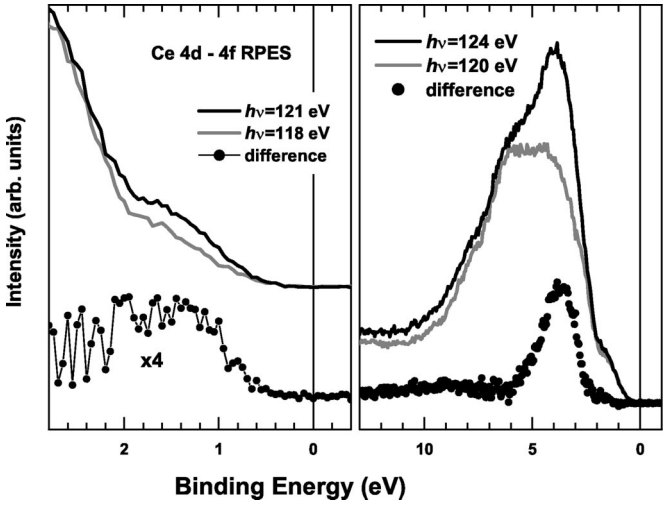

FIG. 4. Left: Comparison of the normalized valence-band PES spectra of LCeMO obtained for $h\nu = 118$ eV and $h\nu = 121$ eV. The difference between these two spectra is shown at the bottom. Right: Similarly for $h\nu = 120$ eV and $h\nu = 124$ eV.

In order to examine the resonating features more clearly, we have compared the valence-band spectra around the two resonating $h\nu$ values of $h\nu \approx 121$ eV and $h\nu \approx 124$ eV. The left panel of Fig. 4 compares the normalized valence-band spectra of LCeMO obtained for $h\nu = 118$ eV and $h\nu = 121$ eV, and the difference between these two spectra is shown at the bottom. Similarly, the right panel compares those for $h\nu = 120$ eV and $h\nu = 124$ eV, and the difference between these two spectra. The left panel shows that the Ce $4f$ contribution is the largest at ~ 1.5 eV below E_F with no Ce $4f$ emission at E_F, consistent with the insulating state above T_C. As mentioned in Fig. 3, the magnitude of the Ce $4f$ resonance at $h\nu \approx 121$ eV is very weak, indicating that the localized Ce $4f$ states are nearly unoccupied in LCeMO and that the Ce valence is far from $3+$. The right panel shows that the O $2p$ states resonate at $h\nu \sim 124$ eV and are spread between ~ 3 and 6 eV BE with no states between E_F and 2 eV BE.

Figure 5 compares the Mn $2p$ XAS spectra of LCeMO and $LaMnO_3$ which was reproduced from Ref. 20. $LaMnO_3$ was chosen as the reference material which has the formally trivalent $(3+)$ Mn ions and the same crystal symmetry. The difference curve between the Mn $2p$ XAS spectrum of LCeMO and that of $LaMnO_3$ is shown at the bottom. The transition metal (T) $2p$ XAS spectrum results from the dipole transitions from the $2p$ core level to the empty $3d$ states. The peak positions and the line shape of the T $2p$ XAS spectrum depend on the local electronic structure of the T ion, which provides the information about the valence state and the ground-state symmetry of the T ion.[21,22] The Mn $2p_{3/2}$ and $2p_{1/2}$ spectral parts are clearly separated by the large $2p$ core-hole spin-orbit interaction.

Similarly as in other manganites,[23] the Mn $2p$ XAS spectra of both LCeMO and $LaMnO_3$ exhibit two broad multi-

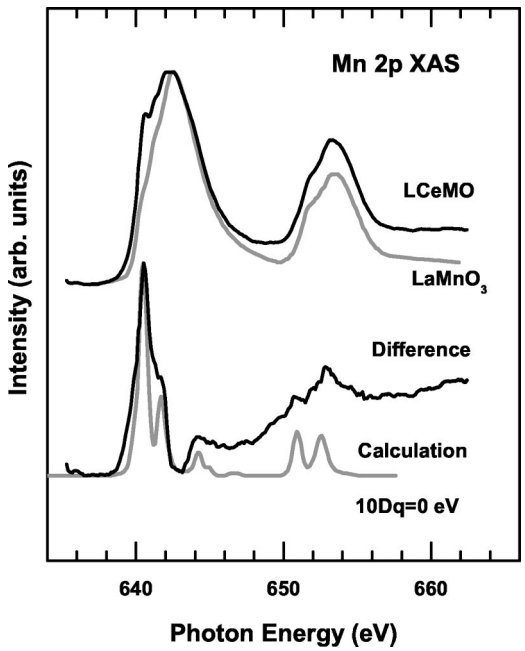

FIG. 5. Comparison of the Mn $2p$ XAS spectra of LCeMO and $LaMnO_3$ (from Ref. 20). The difference curve between the Mn $2p$ XAS spectra of LCeMO and $LaMnO_3$ is shown at the bottom as black lines. The calculated Mn $2p$ XAS spectrum (gray lines) for the Mn^{2+} ion under the O_h symmetry with $10Dq=0$ eV (from Ref. 21) is compared to the difference curve. See the text for the details.

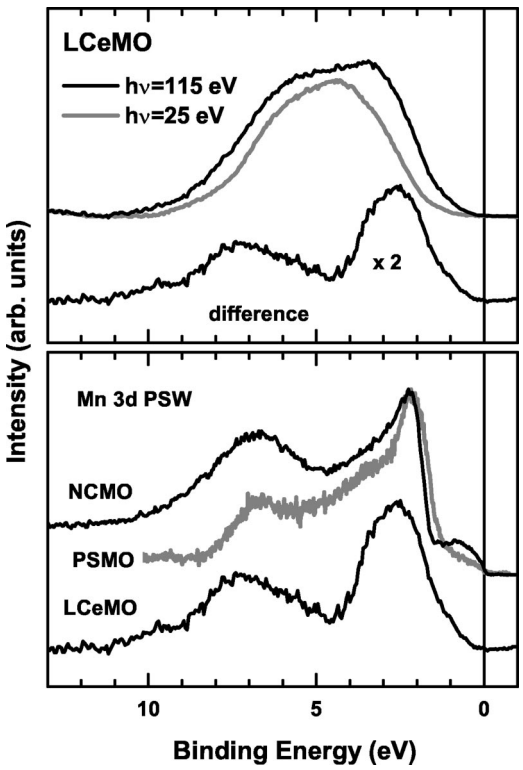

FIG. 6. Top: The extraction procedure for the Mn $3d$ PSW of LCeMO. See the text for the details. Bottom: Comparison of the Mn $3d$ PSW of LCeMO to those of 7%-doped $Nd_{1/2}Ca_{1/2}MnO_3$ (NCMO) (from Ref. 26) and $Pr_{2/3}Sr_{1/3}MnO_3$ (PSMO) (from Ref. 27. The former PSW for NCMO was obtained from the Mn $2p\rightarrow 3d$ RPES. The extraction procedure for the latter PSW for PSMO is described in Ref. 27.

plets separated by the spin-orbit splitting of the Mn $2p$ core hole before subtraction. The main contributions to the broadening come from a large spread of the multiplets[24] and a covalent character of the ground state. In contrast, the difference curve reveals the sharp structure around 640 eV, which resembles that in MnO,[8] indicating the existence of a Mn^{2+} component in LCeMO. To check this argument, we have compared the difference curve to the calculated Mn $2p$ XAS spectrum (gray lines) for the Mn^{2+} ion under the octahedron symmetry (O_h) symmetry with $10Dq=0$ eV. This result has been reproduced from Ref. 21. This comparison clearly shows that the main features of the difference curve can be described mainly with the Mn^{2+} component under the O_h symmetry. Thus Fig. 5 confirms the Mn^{2+}-Mn^{3+} mixed-valent state of Mn ions in LCeMO, in agreement with the previous finding.[8]

The upper panel of Fig. 6 shows the extraction procedure of the Mn 3d partial spectral weight (PSW) of LCeMO. As a first approximation, the Mn $3d$ PSW of LCeMO is determined by subtracting the valence-band spectrum at $h\nu=25$ eV, where the O $2p$ emission is dominant, from that at the off-resonance ($h\nu=115$ eV) in Ce $4d\rightarrow 4f$ RPES, where the Mn $3d$ and O $2p$ emissions are comparable to each other.[5] The former spectrum has been scaled by a factor of ~ 0.9 to account for the $h\nu$ dependence of the O $2p$ photoionization cross section.[25] The extracted Mn $3d$ states show two broad structures, around ~ 2 eV and and ~ 7 eV. The spectral intensity at ~ 1 eV below E_F is weak.

The bottom panel of Fig. 6 compares the Mn $3d$ PSWs of LCeMO to those of $Nd_{0.5}Ca_{0.5}Mn_{0.93}Cr_{0.07}O_3$ (NCMO, Ref. 26) and $Pr_{2/3}Sr_{1/3}MnO_3$ (PSMO, Ref. 27) both of which are metallic in the ground state. The former Mn $3d$ PSW for NCMO was obtained from the Mn $2p\rightarrow 3d$ RPES. The extraction procedure for the latter PSW for PSMO is described in Ref. 27. It was extracted by employing the same procedure as for LCeMO, where $h\nu=119$ eV was used as the off resonance in Pr $4d\rightarrow 4f$ RPES and the $h\nu=18$ eV spectrum was considered as roughly representing the O $2p$ spectrum. Indeed, the Mn $3d$ PSW for PSMO is very similar to that for NCMO, obtained from the Mn $2p\rightarrow 3d$ RPES, except for the slightly lower intensity near E_F. This finding supports the validity of the extraction scheme for the Mn $3d$ PSW employed in this work.

In order to understand the microscopic origin of the valence-band electronic structures of LCeMO, we have compared the experimentally determined Mn $3d$ PSW and O $1s$ XAS spectrum to the calculated Mn $3d$ PDOS, which was obtained from the supercell LSDA+U calculation. The O $1s$ XAS spectrum reflects the transition from the O $1s$ core level to the unoccupied O $2p$ states hybridized to the other electronic states. Therefore the O $1s$ XAS provides a reasonable approximation for representing the unoccupied conduction-band electronic structure. The results are presented in Fig. 7. The parameters used in this calculation are the Coulomb correlation $U=4.0$ eV and the exchange corre-

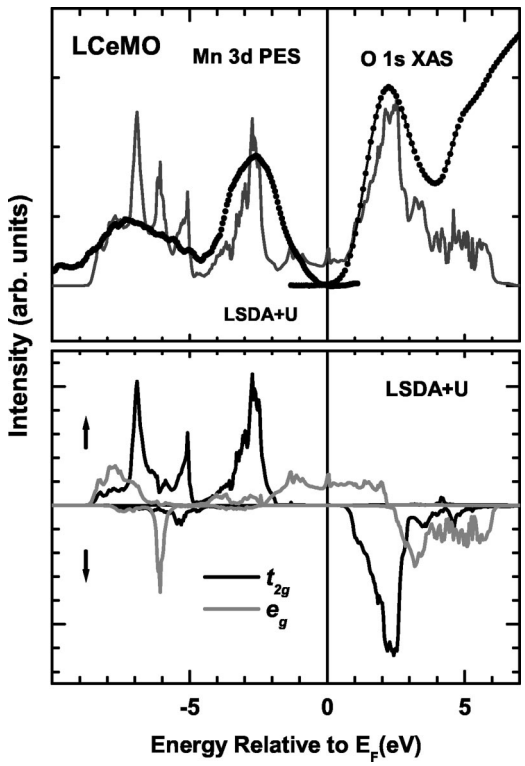

FIG. 7. Top: Comparison of the experimental Mn $3d$ PSW and O $1s$ XAS spectrum and the calculated Mn $3d$ PDOS obtained from the LSDA$+U$ calculation. The O $1s$ XAS spectrum is shifted by referring to the calculated PDOS. Bottom: The calculated Mn $3d$ PDOSs of LCeMO obtained from the LSDA$+U$ calculation. The Mn $3d$ band is decomposed into t_{2g} (black lines) and e_g (gray lines) bands.

lation $J=0.87$ eV for Mn $3d$ electrons, and $U=5.0$ eV and $J=0.95$ eV for Ce $4f$ electrons. It is found that the LSDA $+U$ results are not very sensitive to the U-value, within $\Delta U \approx \pm 1$ eV. As shown at the bottom of Fig. 7, the LSDA $+U$ calculation predicts a half-metallic ground state for LCeMO, which is consistent with the calculated electronic structure obtained in the virtual crystal approximation.[28] In this comparison, the O $1s$ XAS spectrum was shifted so that the peak in the O $1s$ XAS spectrum aligns with that in the LSDA$+U$ calculation.[29] This comparison shows that the measured PES/XAS data for LCeMO agree reasonably well with the calculated Mn $3d$ PDOS, particularly in the peak positions. The broad peak around -3 eV originates from the t_{2g}^3 and e_g^x majority-spin states, and the high BE features (-5–-10 eV) have the strongly mixed electron character of the Mn $3d$-O $2p$ electrons.

The ground state of LCeMO becomes half metallic in the LSDA$+U$ calculation, reflecting that the DE mechanism is still operative in LCeMO.[30] Indeed this prediction is consistent with the recent observation[20] of a large tunneling magnetoresistance (TMR) in ferromagnetic tunnel junction built from LCeMO/$La_{0.7}Ca_{0.3}MnO_3$, which suggests a high degree of spin polarization in LCeMO. The LSDA$+U$ calculation, however, indicates that LCeMO would be a majority-spin carrier half-metal, contrary to a minority-spin carrier half-metal suggested by Ref. 20 based on the large positive TMR. This point remains to be clarified experimentally by employing direct spin-resolved experimental probes.

Finally, the measured spectral weight at E_F $[I(E_F)]$ with respect to the Mn t_{2g} peak is lower than the calculated PDOS at E_F $[N(E_F)]$. This difference near E_F can be ascribed partly due to the measurement temperature being above the M-I transition (≈ 250 K), which corresponds to the insulating phase. The second possibility for this discrepancy is the surface contribution in the measured PES spectra, which were obtained with $h\nu$'s in the rather surface-sensitive regime.[31] Normally surface electronic structures are more insulating than the bulk electronic structure due to the more localized nature of the electrons at the surface. The third possibility for this discrepancy is the presence of some kind of carrier localization mechanism. Several mechanisms have been reported to explain the pseudogap nature in manganites.[32] Assuming that the Coulomb correlation between Mn $3d$ electrons is properly accounted for by the LSDA$+U$ method,[33] one of the plausible localization mechanisms would be the small polaron formation induced by the strong e_g electron-phonon interaction, originating from the Jahn-Teller active Mn^{3+} ion in LCeMO.[27,34]

IV. CONCLUSION

We have performed PES and XAS measurements for LCeMO thin film, including the RPES measurement near the Ce $4d \rightarrow 4f$ absorption edge, and the XAS measurements near the Ce and La $3d$, Mn $2p$, and O $1s$ absorption edges. The PES and XAS data have been compared to the band-structure calculations performed in the LSDA$+U$ method. Both the Ce $3d$ core-level PES and XAS spectra are very similar to those of CeO_2 with Ce^{4+}, indicating that the Ce valence is far from $3+$ in LCeMO. The RPES measurement also shows very weak enhancement around the Ce $4d \rightarrow 4f$ absorption edge, providing evidence that the localized Ce $4f$ states are almost empty in the ground state. The Mn $2p$ XAS spectrum reveals the multiplet features of Mn^{2+} ions besides those of Mn^{3+} ions, confirming the existence of the Mn^{2+}-Mn^{3+} mixed-valent states of Mn ions in LCeMO. This study confirms that the LCeMO films are indeed electron doped. The comparison between the measured Mn $3d$ PES/XAS data and the calculated Mn $3d$ PDOS in the LSDA$+U$ method shows a reasonably good agreement, particularly in the peak positions. The LSDA$+U$ calculation predicts a half-metallic ground state for LCeMO with majority spin carriers at E_F. However, the predicted half-metallic ground state is not observed in the PES measurement done above the M-I transition temperature.

ACKNOWLEDGMENTS

This work was supported by the KRF (Grant No. KRF–2002-070-C00038) and by the KOSEF through the CSCMR at SNU and the eSSC at POSTECH. The PAL is supported by the MOST and POSCO in Korea.

*Author to whom correspondence should be addressed. Email address: kangjs@catholic.ac.kr

[1] S. Jin, T.H. Tiefel, M. McCormack, R.A. Fastnacht, R. Ramesh, and L.H. Chen, Science **264**, 413 (1994).
[2] C. Zener, Phys. Rev. **82**, 403 (1951).
[3] P. Mandal and S. Das, Z. Phys. B: Condens. Matter **104**, 7 (1997); Phys. Rev. B **56**, 15 073 (1997).
[4] J.R. Gebhardt, S. Roy, and N. Ali, J. Appl. Phys. **85**, 5390 (1999).
[5] J.-S. Kang, Y.J. Kim, B.W. Lee, C.G. Olson, and B.I. Min, J. Phys.: Condens. Matter **13**, 3779 (2001).
[6] P. Raychaudhuri, S. Mukherjee, A.K. Nigam, J. John, U.D. Vaisnav, R. Pinto, and P. Mandal, J. Appl. Phys. **86**, 5718 (1999).
[7] C. Mitra, P. Raychaudhuri, J. John, S.K. Dhar, A.K. Nigam, and R. Pinto, J. Appl. Phys. **89**, 524 (2001).
[8] C. Mitra, Z. Hu, P. Raychaudhuri, S. Wirth, S.I. Csiszar, H.H. Hsieh, H.-J. Lin, C.T. Chen, and L.H. Tjeng, Phys. Rev. B **67**, 092404 (2003).
[9] S.K. Kwon and B.I. Min, Phys. Rev. Lett. **84**, 3970 (2000).
[10] E. Wuilloud, B. Delley, W.-D. Schneider, and Y. Baer, Phys. Rev. Lett. **53**, 202 (1984).
[11] C. Suzuki, J. Kawai, M. Takahashi, A.M. Vlaicu, H. Adachi, and T. Mukoyama, Chem. Phys. **253**, 27 (2000).
[12] S. Doniach and M. Sǔnjic, J. Phys. C **3**, 285 (1970).
[13] A. Fujimori Phys. Rev. B **28**, 2281 (1983); **28**, 4489 (1983).
[14] A. Kotani and H. Ogasawara, J. Electron Spectrosc. Relat. Phenom. **60**, 257 (1992).
[15] The intensity of each peak is proportional to square of the overlap integral between the initial and final states.
[16] G. Kaindl, G. Kalkowski, W.D. Brewer, B. Perscheid, and F. Holtzberg, J. Appl. Phys. **55**, 1910 (1984).
[17] C.G. Olson, S.J. Chase, P. Canfield, and D.W. Lynch, J. Electron Spectrosc. Relat. Phenom. **93**, 175 (1998).
[18] J.W. Allen, J. Magn. Magn. Mater. **47-48**, 168 (1985).
[19] F. Gerken, Ph.D. thesis, University of Hamburg, Germany.
[20] C. Mitra, P. Raychaudhuri, K. Dörr, K.-H. Müller, L. Schultz, P.M. Oppeneer, and S. Wirth, Phys. Rev. Lett. **90**, 017202 (2003).
[21] F.M.F. de Groot, J.C. Fuggle, B.T. Thole, and G.A. Sawatzky, Phys. Rev. B **42**, 5459 (1990).
[22] G. van der Laan and I.W. Kirkman, J. Phys.: Condens. Matter **4**, 4189 (1992).
[23] J.-H. Park, C.T. Chen, S-W. Cheong, W. Bao, G. Meigs, V. Chakarian, and Y.U. Idzerda, Phys. Rev. Lett. **76**, 4215 (1996).
[24] T. Saitoh, A.E. Bocquet, T. Mizokawa, H. Namatame, A. Fujimori, M. Abbate, Y. Takeda, and M. Takano, Phys. Rev. B **51**, 13 942 (1995).
[25] J.J. Yeh and I. Lindau, At. Data Nucl. Data Tables **32**, 1 (1985).
[26] J.-S. Kang, J.H. Kim, A. Sekiyama, S. Kasai, S. Suga, S.W. Han, K.H. Kim, E.J. Choi, T. Kimura, T. Muro, Y. Saitoh, C.G. Olson, J.H. Shim, and B.I. Min, Phys. Rev. B **68**, 012410 (2003).
[27] J.-S. Kang, C.G. Olson, J.H. Jung, S.T. Lee, T.W. Noh, and B.I. Min, Phys. Rev. B **60**, 13 257 (1999).
[28] B.I. Min, S.K. Kwon, B.W. Lee, and J.-S. Kang, J. Electron Spectrosc. Relat. Phenom. **114**, 801 (2001).
[29] The O 1*s* XAS spectrum was shifted by -527.5 eV. There is some uncertainty in choosing the zero position from the XAS spectrum.
[30] The supercell calculation in the LSDA yields the normal metallic LCeMO, contrary to the LSDA$+U$ result. This implies that including the U effect is essential to describe the half-metallic nature of LCeMO.
[31] J.-S. Kang, J.H. Kim, A. Sekiyama, S. Kasai, S. Suga, S.W. Han, K.H. Kim, T. Muro, Y. Saitoh, C. Hwang, C.G. Olson, B.J. Park, B.W. Lee, J.H. Shim, J.H. Park, and B.I. Min, Phys. Rev. B **66**, 113105 (2002).
[32] See, for example, E. Dagotto, T. Hotta, and A. Moreo, Phys. Rep. **344**, 1 (2001).
[33] Note, however, that the LSDA$+U$ method is only a static approximation of the self-energy, and the dynamical contribution of the self-energy is totally neglected. Furthermore, the Coulomb interaction parameter is not determined in a first-principle way.
[34] J.D. Lee and B.I. Min, Phys. Rev. B **55**, 12 454 (1997).